International Journal of Bifurcation and Chaos, Vol. 20, No. 11 (2010) 3717–3723

DOI: 10.1142/S0218127410027982

SELF-AVOIDING CHIRAL WALKS

SUMANA DUTTA and OLIVER STEINBOCK*
Florida State University,
Department of Chemistry and Biochemistry,
Tallahassee, FL 32306-4390, USA
**steinbck@chem.fsu.edu*

Received January 28, 2010

We describe a simple, discrete model of deterministic chiral motion on a square lattice. The model is based on rotating walkers with trailing tails spanning L lattice bonds. These tail segments cannot overlap and their leading A segments cannot be crossed. As prescribed by their chirality, walkers must turn if possible, or go straight, or else correct earlier steps recursively. The resulting motion traces unbound trajectories and complex periodic orbits with various symmetries. Periods tend to decrease with increasing L and vary between L and L^2. Interacting walkers can form intricate pair states. Some orbits match pinned spiral tip trajectories observed experimentally in excitable systems.

Keywords: Cellular automaton; spiral wave; excitable system; self-avoiding walk.

1. Introduction

Throughout science and mathematics, chirality is an important property. It implies that a geometrical object, particle or structure cannot be mapped to its mirror image by rotations and translations alone. Examples include certain knots, enantiomers such as chiral drugs, vortex patterns, elementary particles, and human hands [Saito *et al.*, 2006; Kondepudi *et al.*, 1990]. Symmetry breaking in these diverse systems has attracted considerable scientific interest revealing profound insights into our universe. However, the question as to how chiral building blocks and/or chiral dynamics affect the symmetries of derived phenomena is by comparison understudied. Nonetheless, there are numerous interesting examples of inherited chirality such as the macroscopic shapes of bacterial colonies that reflect the microscopic chiralilty of flagella [Ben-Jacob *et al.*, 1995]. Similarly there are close links between molecular chirality and pattern formation in liquid crystals, Langmuir monolayers, smectic films [Selinger *et al.*, 1993; de Gennes, 1974] and molecular chiral superstructures [Staneic *et al.*, 2006; Pokroy *et al.*, 2009]. In this article, we describe and investigate a very simple model of chiral dynamics. The model is closely related to the rotation of spiral waves in excitable systems such as the Belousov–Zhabotinsky (BZ) reaction. These vortices are known to pin to impenetrable and unexcitable obstacles [Steinbock & Müller, 1992]. In obstacle arrays that confine the excitable medium to a square network, the central spiral tip rotates along intricate trajectories that encompass numerous obstacle units [Ginn & Steinbock, 2004, 2005]. A typical example is shown in Fig. 1. Here the excitation spiral (white regions) is strongly fragmented due to the externally imposed geometry and also deformed as the overall wave propagation is unobstructed only along the straight horizontal and vertical channels. More importantly, the spiral tip rotates steadily around a linear chain of three next-neighbor obstacles (marked with "x" in figure).

In general, these periodic orbits depend critically on the ratio between the obstacle perimeter Λ

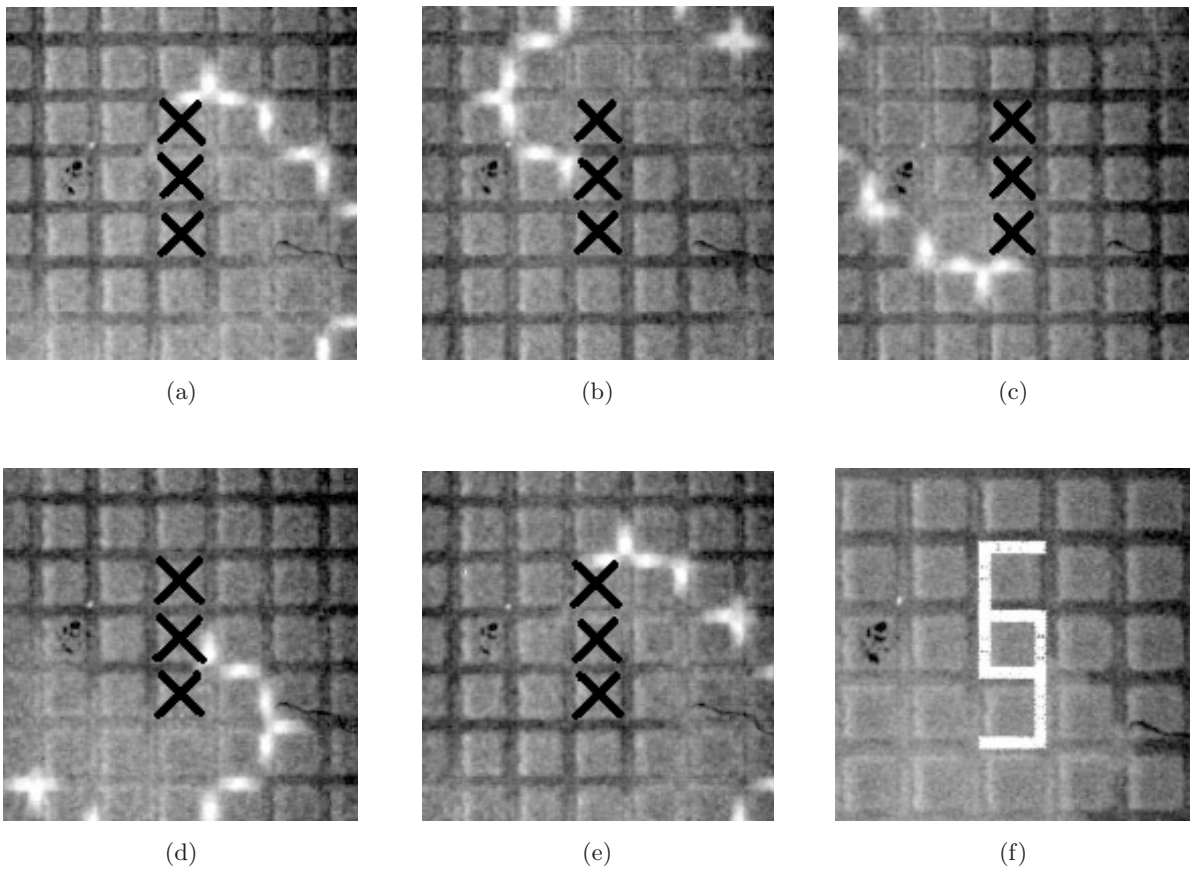

Fig. 1. (a)–(e) Five consecutive snapshots of a spiral wave in a BZ reaction medium confined to a Manhattan-like network. The excitable tracks appear as a dark grid. The enclosed squares are nonreactive elastomer obstacles produced by soft-lithography. The spiral tip rotates around 1×3 obstacle units (marked by black crosses). The time elapsed between subsequent frames is 75 s. Frame (f) shows the resulting tip trajectory. See reference [Ginn & Steinbock, 2004] for additional details.

and the length of the refractory zone λ on the back of the excitation pulse [Tamarit *et al.*, 1996]. If $\lambda < \Lambda$ then the tip rotates around a single obstacle unit. Otherwise, rotation must occur around a minimum of two next-neighbor obstacles because the spiral encounters its own refractory tail. In this process, the tip periodically enters connecting channels but fails to exit, vanishes and the next closest wave segment becomes the primary pacemaker. Notice that many other complex orbits have been observed in chemical experiments and reaction–diffusion models including trajectories generated by repeating sequences such as $\overline{\mathrm{TTTS}}$ (2×2 obstacle box) and $\overline{\mathrm{TSTST}}$ (cross of five obstacles), where "T" and "S" indicate turns and straight moves, respectively. Lastly, we emphasize that these "semi-discrete" excitable media have been attracting considerable interest in recent years. In addition to the elastomer-based microreactor in Fig. 1, such experiments involve, for instance, catalyst patterns printed onto specialized membranes [Steinbock *et al.*, 1995] as well as microfluidic assemblies of immiscible fluids [Toiya *et al.*, 2008].

2. The Model

Our model aims to capture the fundamental aspects of pinned spiral tips or similar chiral motion in the form of a deterministic walker on a square lattice. The walker moves forward at a speed of one lattice bond per iteration and turns clockwise whenever possible. In addition, the walker has a continuous tail which represents the refractory zone or a similar object. The tail has a constant length of L lattice bonds (in the following called segments). An overlapping of tail segments is forbidden, i.e. each lattice bond can be occupied by only one tail segment at a time. In addition, the leading A ($0 \leq A \leq L$) segments of the tail show "absolute refractoriness" and their endpoints cannot be crossed by the walker. The working rules to advance the walker from iteration t to $t + 1$ are: (1) walker

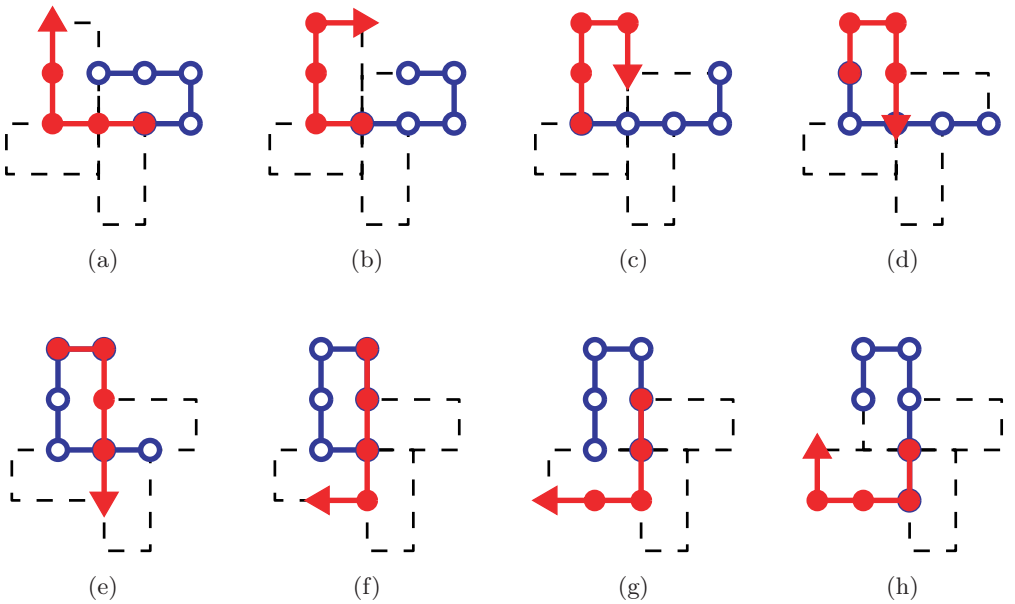

Fig. 2. Stepwise dynamics of a tailed chiral walker. The leading $A = 4$ tail segments involve five lattice nodes that cannot be crossed (red lines and solid symbols). The $R = 4$ rear segments (blue lines) cannot overlap with other segments but their four nodes (blue open circles) can be crossed. The dashed line is the periodic orbit of the walker. An animation (movie 2) is also provided.

turns clockwise if possible; (2) or else the walker goes straight if possible; (3) otherwise the system is reset recursively to iteration $t - \tau$ (starting at $\tau = 1$). If the walker had turned in that iteration, this turn is replaced by a straight step and iterations continue from the corrected iteration time $(t - \tau)$ (see movie 1). We emphasize that these walkers never turn counter-clockwise and, thus, have a conserved chirality of $X = +1$. The motion of counter-clockwise rotating walkers ($X = -1$) is analogous to their mirror-image counterparts. Notice that the employed recursive correction is similar to the vanishing of a spiral tip segment and the promotion of another to primary pacemaker.

Figure 2 shows a sequence of eight consecutive iterations for a tailed chiral walker with $L = 8$ and $A = 4$. The arrow indicates the head of the walker. The solid (red) and open (blue) circles along with their connecting lines (same colours) represent the absolute refractory tail and the trailing $R = L - A$ segments, respectively. If the walker starts from a fully elongated initial condition, it requires only nine iterations to reach a periodic state. The trajectory of this state is shown as dashed lines in Fig. 2. Using two-dimensional point group nomenclature [Mezey, 1991], it is a chiral pattern with C_4 symmetry and its period is 24. The specific steps in Fig. 2 are: turn from (a) to (b) and (b) to (c), straight from (c) to (d) because the target node for the turn shows absolute refractoriness, straight from (d) to (e) because the target bond for the turn is occupied, turn from (e) to (f), straight from (f) to (g) because the turn would jam the walker in the next iteration, and turn from (g) to (h). Notice that patterns (a) and (g), which are separated by six steps, can be matched by a 90° rotation. This feature accounts for the observed period and four-fold symmetry of the orbit.

3. Results and Discussions

A survey for all $L \leq 100$ and $A \leq 50$ revealed that every walker in this range of parameter values converges to a periodic state if started from a fully straight initial condition. The phase diagram in Fig. 3 shows the corresponding orbits for a smaller range of A and R values. No orbit is unique to a particular point in the phase diagram as the pattern for (A, R) is always identical to the one for $(A+1, R-1)$ or an even larger, connected region in the phase diagram. Accordingly, we partition Fig. 3 into equal-orbit domains using thin horizontal and vertical lines. The characteristic orbits are superimposed and small patterns are magnified for clarity. Some trajectories are unbound states for which the walker moves in diagonal directions or along the lattice lines (see movie 3). The corresponding patterns are labeled with small markers and are plotted in red.

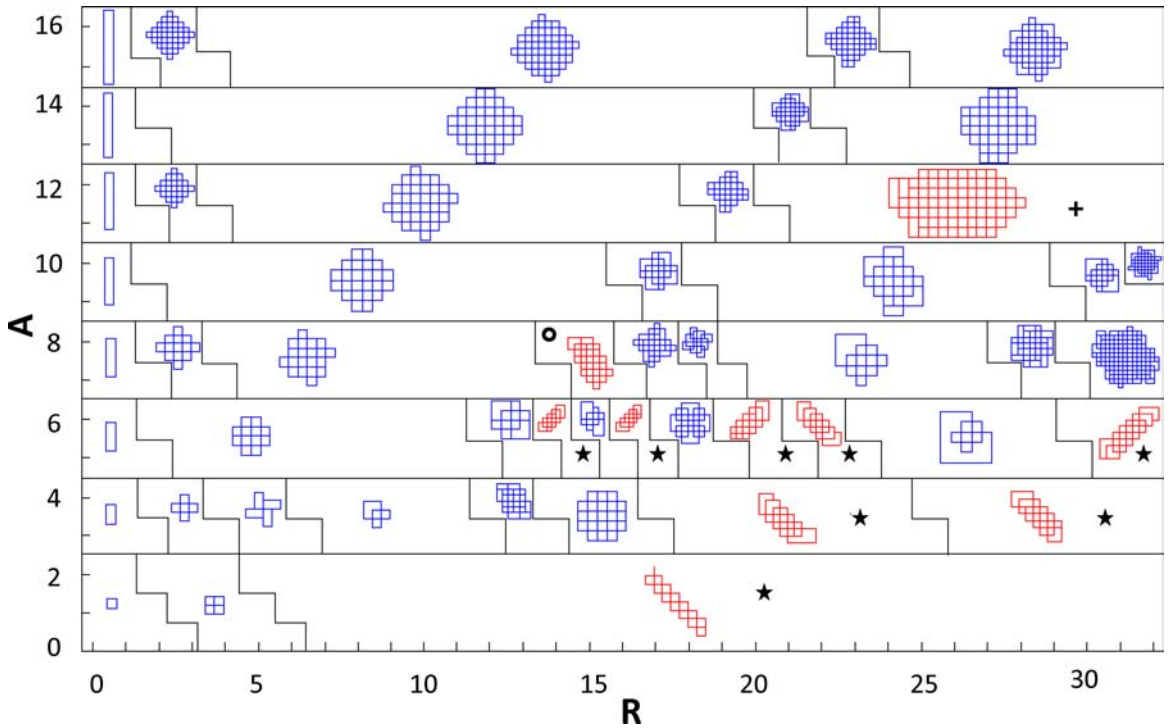

Fig. 3. Phase diagram of chiral walker motion segmented into regions of identical trajectories. The parameters R and A denote the length of the relative and the absolute refractory tail, respectively. Unbound states are plotted in red and are labeled with a plus sign (drift along lattice lines), an asterisk (drift in 45° direction), or a circle (30° direction).

We emphasize that in these cases the walker is still periodic. For example, all walkers with $A < 3$ and $R > 6$ move by repeating the sequence $\overline{\text{STSTTT}}$. Also notice that the two-dimensional symmetries of the orbits in Fig. 3 include C_2, C_4, D_2 and D_4. An instance of C_1 symmetry is found to exist for $(A, R) = (7, 36)$. Examples for each of these cases are shown in Fig. 4. Another characteristic feature of the phase diagram is that, with the exception of $A = 0, 1, 2$, all domains have a height of two A units, or more precisely, consist of an odd and a by one larger, even A value. In addition, non-horizontal domain boundaries always follow constant L values and are, hence, step-shaped.

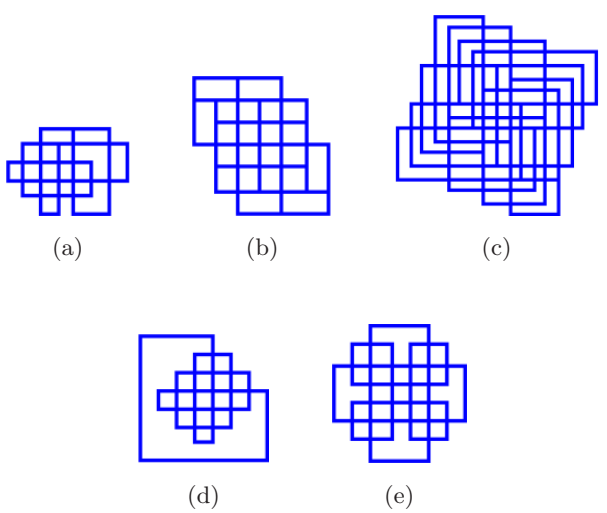

Fig. 4. Orbits having (a) C_1, (b) C_2, (c) C_4, (d) D_2 and (e) D_4 symmetries. The corresponding parameter values (A, R) are $(7, 36)$, $(3, 14)$, $(22, 98)$, $(10, 50)$, $(5, 19)$, respectively.

An important question concerns the dependence of the periodic orbits on the initial condition of the walker. For $L < 15$, we tested all initial shapes that (i) do not reuse lattice bonds and (ii) do not cause immediate jamming. Notice that the number of paths selected by (i) scales exponentially with L [Guttmann, 1985]. Disregarding differences in absolute position and orientation, we find no dependence on the initial condition. Only the patterns for $R \leq 2$ (cf. Fig. 3) vary between rectangles of different width but equal perimeter and period. We emphasize that we did not find any walkers without periodic (or drifting) solution. Clearly, we currently cannot rule out more complicated behavior for very long walkers. Hence, notice that all subsequent results are obtained for initially linear walkers.

Surprisingly, the period T of chiral walkers tends to *decrease* with increasing tail lengths L

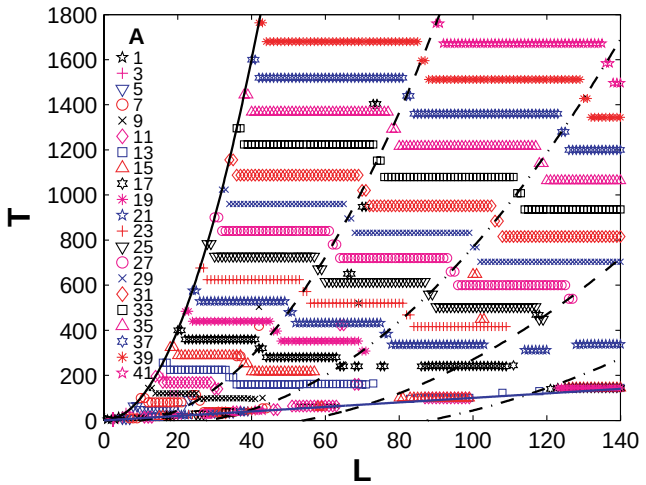

(a)

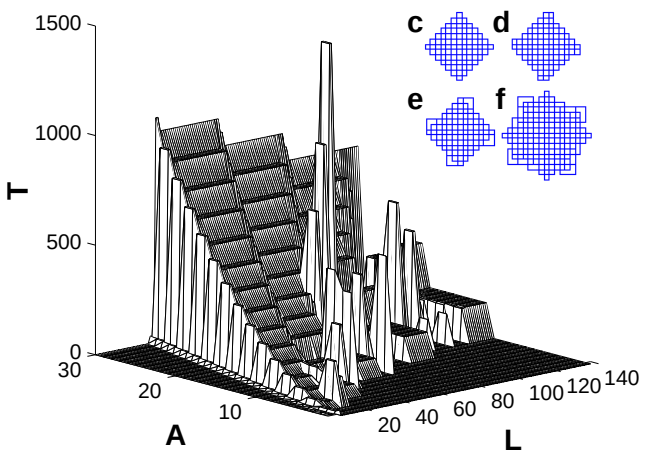

(b)

Fig. 5. (a) Period of nondrifting walkers as a function of the tail length L. Plot symbols correspond to different values of A as specified in the legend. The black curves are the parabolas $p = 1$–5 specified in Eq. (1). The continuous blue line is lower bound $T = L$. (b) Period as a function of A and L. (c)–(e) Periodic orbits for $A = 23$ as found for the intersections with parabolas $p = 1$–3 in (a). (f) Periodic orbit for $(A, L) = (17, 75)$ which corresponds to the largest spike in (b).

but increases with increasing A. Here, we define the period as the smallest number of iterations required for reestablishing the absolute positions of all tail segments. Data from drifting walkers are, hence, not included. Figure 5(a) shows $T(L)$ for all A values less than 43. The different A values are distinguished by plot symbol and color. For large A, the dependence can be described as a sequence of decreasing plateaus separated by pairs of intermediate periods. The data in Fig. 5(a) suggests that the plateau-connecting pairs describe parabolas of the form

$$T_p(L) = \frac{1}{p^2}[L - (2p-2)][L - (2p-2)(2p+1)], \tag{1}$$

where $p \in \mathbb{N}^*$ indexes the parabolas in the direction of increasing L. The first five parabolas ($p \leq 5$) are shown in Fig. 5(a). Notice that $T_1(L) = L^2$ is the maximum period for walkers with tail length L. The corresponding orbits are simple diamonds of height $(A_{\text{even}} + 2)/2$ or $(A_{\text{odd}} + 3)/2$ [e.g. Fig. 5(c)]. In addition, walkers must have periods greater or equal to L because no orbit can consist of fewer than L bonds. In Fig. 5(a), this lower bound is plotted as a solid blue line. The parabolas in combination with the $T = L$ curve seem to be important for determining L-dependent changes in the period of the walkers. More specifically, we find that these changes tend to occur when a plateau intersects with any of these curves.

Most of the aforementioned plateaus have a unique period. However, there are some exceptions such as for $A = 13$ where the second highest level varies by two time steps. Moreover, there are two interesting degeneracies. First, two neighboring points in a plateau can have the same period but differently shaped orbits. Second, identical orbits can have slightly different periods. Simple examples of these two cases are $(A, R) = (5, 12), (5, 13)$ and $(A, R) = (5, 4), (5, 5)$, respectively. We emphasize that for the parameter range investigated these scenarios are exceptions.

At intermediate A values, we find a similar plateau structure but some isolated data points and pairs fail to obey this simple pattern. For unknown reasons, these exceptions are quite pronounced for $A = 17$. As illustrated in Fig. 5(b), the situation is overall more complex for small A values. Notice that $T = 0$ indicates drifting walkers (and the ill-defined parameter region $A > L$). Consequently, Fig. 5(b) suggests that drift occurs for small A values while the plateau theme governs periods for large A. For intermediate values, we find a complex dependence of the period on the system parameters. Some parameter pairs have periods that are surprisingly larger than the periods in their immediate neighborhood. The corresponding orbits, however, show no unusual features [Fig. 5(f)].

In the following, we consider the case of interacting chiral walkers. All rules for single walkers are upheld and generalized in the obvious sense that walkers must neither overlap with any other

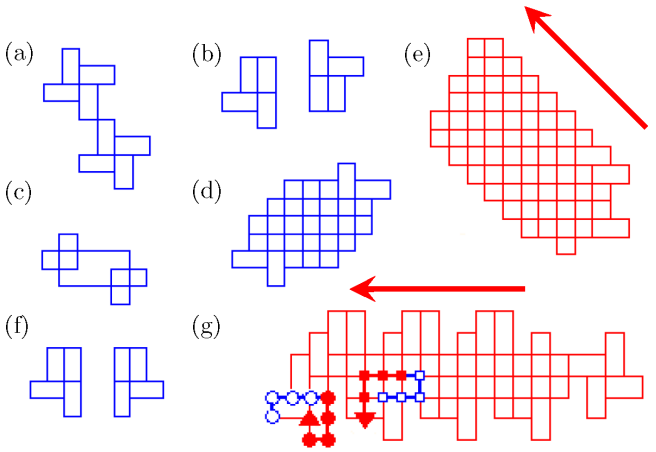

Fig. 6. Orbits of walker pairs with $L_{1,2} = 8$ and $A_{1,2} = 4$. Chiralities in (a)–(e) are $X_{1,2} = +1$ and $(X_1, X_2) = (+1, -1)$ in (f), (g). The pairs in (e), (g) are unbound and move in directions indicated by the arrows. All walkers were initially straight and parallel, but their relative distance d and their offset in tail direction h varied: $(d, h) = (3, 0)$ in (a), $(1, 0)$ in (b, g), $(2, 0)$ in (c, f), $(3, 1)$ in (d), and $(2, 2)$ in (e). Also see movie 4.

walkers' tail nor cross nodes that are absolute refractory. In addition, we require one new rule to resolve the behavior in head-on collisions. To avoid such a situation, we change *both* involved walkers from "T" to "S" or else correct by recursion. Moreover, we allow the walkers to have different chirality X.

In contrast to solitary walkers, pair dynamics strongly depend on the specific initial conditions. Overall the dynamics can be grouped into three different categories: (1) The walkers are sufficiently far apart and move along their characteristic, single-walker orbits. (2) The latter orbits touch or even overlap, but there is no interaction due to temporal separation. This situation is mainly relevant for walkers with equal period. (3) Pair-specific orbits which differ qualitatively from the single-walker orbits form and are either localized or unbound.

Figure 6 shows seven examples for a walker pair with $(L, A) = (8, 4)$. Both walkers move clockwise in (a)–(e) while they rotate in opposite directions in (f) and (g). The differences between the trajectories (a)–(e) and (f), (g) result only from small differences in the initial condition (see caption). Many of the trajectories observed for periodic pair motion [e.g. Fig. 6(c)] are not found for any solitary walker. They include chiral as well as achiral patterns [e.g. Figs. 6(b) and 6(f)]. Moreover, we find a range of periods associated with the different pair solutions. For the states in Fig. 6, these periods are 24 in (a), (b), and (f), 28 in (c), and 120 in (d).

The dependence of multiwalker systems on their initial conditions greatly increases the complexity of our model, thus, making it highly challenging for computational analyses. Qualitatively, however, our results suggest that interacting walkers of opposite chirality often form drifting pair states if they do not decouple early on. The simplest example for a translational motion involves two heads that are aligned and, hence, always move straight to avoid a head-on collision. However, we also find highly intricate drift patterns in which the individual walkers perform complex, individual step sequences. Clearly more work is needed to describe multiwalker dynamics including collisions involving drifting walkers, some of which might be reminiscent of the complex behavior in cellular automata such as Conway's "Life".

4. Conclusions

In conclusion, we have proposed a set of simple rules governing the deterministic motion of tailed chiral walkers on a square lattice. The leading part of the tail is fully self-avoiding while the trailing part is weakly self-avoiding [Domb, 1983; Kennedy, 1994]. This combination of lattice bond and lattice node rules is important for the model's complexity as only very simple orbits are found for $A = 0$ or $R = 0$. Furthermore, the tail shares similarities with the refractory zone of rotating excitation waves. Accordingly, we find that some chiral walkers describe periodic orbits that are also observed in experiments and simulations with pinned spiral waves in the Belousov–Zhabotinsky reaction.

Acknowledgments

This material is based on work supported by the National Science Foundation under Grant No. 0513912.

References

Ben-Jacob, E., Cohen, I., Shochet, O., Tenenbaum, A., Czirók, A. & Vicsek, T. [1995] "Cooperative formation of chiral patterns during growth of bacterial colonies," *Phys. Rev. Lett.* **75**, 2899–2902.

de Gennes, P. G. [1974] *The Physics of Liquid Crystals* (Oxford University Press, London).

Domb, C. [1983] "From random to self-avoiding walks," *J. Stat. Phys.* **30**, 425–436.

Ginn, B. T. & Steinbock, O. [2004] "Quantized spiral tip motion in excitable systems with periodic heterogeneities," *Phys. Rev. Lett.* **93**, 158301(1-4).

Ginn, B. T. & Steinbock, O. [2005] "Front aggregation in multiarmed excitation vortices," *Phys. Rev. E* **72**, 046109(1-4).

Guttmann, A. J. [1985] "Lattice trails. I. Exact results," *J. Phys. A* **18**, 567–573.

Kennedy, T. [1994] "Ballistic behavior in a 1D weakly self-avoiding walk with decaying energy penalty," *J. Stat. Phys.* **77**, 565–579.

Kondepudi, D. K., Kaufman, R. J. & Singh, N. [1990] "Chiral symmetry breaking in sodium chlorate crystallizaton," *Science* **250**, 975–976.

Mezey, P. G. [1991] *New Developments in Molecular Chirality* (Kluwer Academic Publishers, Dordrecht).

Pokroy, B., Kang, S. H., Mahadevan, L. & Aizenberg, J. [2009] "Self-organization of a mesoscale bristle into ordered, hierarchical helical assemblies," *Science* **323**, 237–240.

Saito, H., Kawaguchi, Y. & Ueda, M. [2006] "Breaking of chiral symmetry and spontaneous rotation in a spinor Bose–Einstein condensate," *Phys. Rev. Lett.* **96**, 065302(1-4).

Selinger, J. V., Wang, Z. G., Bruinsma, R. F. & Knobler, C. M. [1993] "Chiral symmetry breaking in Langmuir monolayers and smectic films," *Phys. Rev. Lett.* **70**, 1139–1142.

Staniec, P. A., Perdigão, L. M. A., Rogers, B. L., Champness, N. R. & Beton, P. H. [2006] "Honeycomb networks and chiral superstructures formed by cyanuric acid and melamine on Au(111)," *J. Phys. Chem. C* **111**, 886–893.

Steinbock, O. & Müller, S. C. [1992] "Chemical spiral rotation is controlled by light-induced artificial cores," *Physica A* **188**, 61–67.

Steinbock, O., Kettunen, P. & Showalter, K. [1995] "Anisotropy and spiral organizing centers in patterned excitable media," *Science* **269**, 1857–1860.

Tamarit, F. A., Stariolo, D. A., Cannas, S. A. & Serra, P. [1996] "Effects of refractory periods in the dynamics of a diluted neural network," *Phys. Rev. E* **53**, 5146–5152.

Toiya, M., Vanag, V. K. & Epstein, I. R. [2008] "Diffusively coupled chemical oscillators in a microfluidic assembly," *Angew. Chem. Int. Ed.* **47**, 7753–7755.